Effects of Residual Stress on Nano-Mechanical Behavior of Thin Films

M. Sebastiani, E. Bemporad, N. Schwarzer and F. Carassiti

Abstract In this chapter, we present an overview of an optimized method for the determination of surface elastic residual stress in thin ceramic coatings by instrumented sharp indentation. The methodology is based on nanoindentation testing on focused ion beam (FIB) milled micro-pillars. Finite element modeling (FEM) of strain relief after FIB milling of annular trenches demonstrates that full relaxation of pre-existing residual stress state occurs when the depth of the trench approaches the diameter of the remaining pillar. Under this assumption, the average residual stress present in the coating can be calculated by comparing two different sets of load-depth curves: the first one obtained at the center of stress-relieved pillars, the second one on the undisturbed (residually stressed) surface. The influence of substrate's stiffness and pillar's edges on the indentation behavior can be taken into account by means of analytical simulations of the contact stress distributions. Finally, the effect of residual stress on fracture toughness and deformation modes of a TiN PVD coating is analyzed and discussed here.

1 Introduction

Intrinsic (or residual) stresses (Korsunsky 2009; Withers and Bhadeshia 2001), resulting from manufacturing or processing steps, mostly define the performance and limit the lifetime of nanostructured materials (Dye et al. 2001), thin films (Bemporad et al. 2007, 2008; Bull 2005; Bull and Berasetegui 2006; Dye et al. 2001; Espinosa et al. 2003; Fischer et al. 2005; Pauleau 2001; Roy and Lee 2007),

M. Sebastiani (✉) · E. Bemporad · F. Carassiti
Mechanical and Industrial Engineering Department, University of Rome "ROMA TRE",
Via della Vasca Navale 79, 00146 Rome, Italy
e-mail: seba@stm.uniroma3.it

N. Schwarzer
Saxonian Institute of Surface Mechanics, SIO, Tankow 1, 18569 Ummanz, Rügen, Germany

coatings and MEMS devices (Espinosa et al. 2003) and bulk metallic glasses (Wang et al. 2011). The importance of residual stress for micro-systems is relatively more important than in case of conventional materials and structures, due to the size effects in crystal plasticity, fatigue and fracture behavior that have been recently observed for a wide range of materials.

It has been widely reported in the literature that residual stress can affect significantly the adhesion and fracture toughness of thin films for a variety of industrial applications, ranging from wear resistance coatings to thin films for Solid Oxide Fuel Cells (SOFC) and coatings for biomedical applications.

They can also affect load bearing capacity, elastic strain to failure and ductility of Bulk Metallic Glasses (BMGs), the reliability of micro-welds and other metal interconnects, crack propagation and charge carrier mobility in semiconductor BEoL systems with ultra-low-k (ULK) nano-porous films (Ye et al. 2006), and the resonant frequency and lifetime of micro/nano-electro-mechanical systems (MEMS/NEMS) (Bull 2005).

In the specific case of hard nanostructured coatings (Bemporad et al. 2007; Pauleau 2001; Teixeira 2002), strong compressive in-plane stresses is usually observed (both due to the growth process and from different thermal expansion coefficients between coating and substrate (Bemporad et al. 2007), which often involve buckling of the coating or interfacial failure under in-service load conditions.

Notwithstanding these industrial requirements, the evaluation of the residual stress in (sub)micron layers is still an extremely challenging task from a metrology perspective, especially in the case of nano-crystalline, strongly textured, complex multiphase or amorphous materials and thin films.

For such reasons, the development of site-specific micro-scale evaluation techniques of residual stress still represents a critical issue for design and characterization of small scale systems.

However, the established techniques for micron-scale measurement of residual stress still have strong limitations, e.g. in terms of spatial resolution, lack of depth sensing, their applicability on non-crystalline materials or accessibility to industry.

Strong efforts are also needed in the sense of developing a portable and flexible semi-destructive method that would be applicable down to the microscopic scale, and would allow routine determination of residual stress with high spatial resolution (Bolshakov et al. 1996; Suresh and Giannakopoulos 1998; Tsui et al. 1996).

The aim of this work was to develop an effective and reproducible methodology for the assessment of residual stress by the use of sharp nanoindentation testing on a (sub)micron scale (Oliver and Pharr 1992, 2004).

A brief review of the currently available methods for residual stress analysis by nanoindentation is presented (Suresh and Giannakopoulos 1998), whose principle is depicted in Fig. 1.

It is shown that the available methods are affected by a major limitation, consisting of the difficulty in determining the load–displacement curve for the stress-free condition in case of thin films.

Fig. 1 Concept of residual stress analysis by sharp indentation. **a** a tensile residual stress induces a more pronounced sinking-in with respect to the contact profile corresponding to the stress-free state; **b** a compressive stress induces a piling-up; **c** in both cases, a deviation of the load–displacement curve with respect to the stress-free state is observed, due to the modification of the contact area described by Eqs. (1–2)
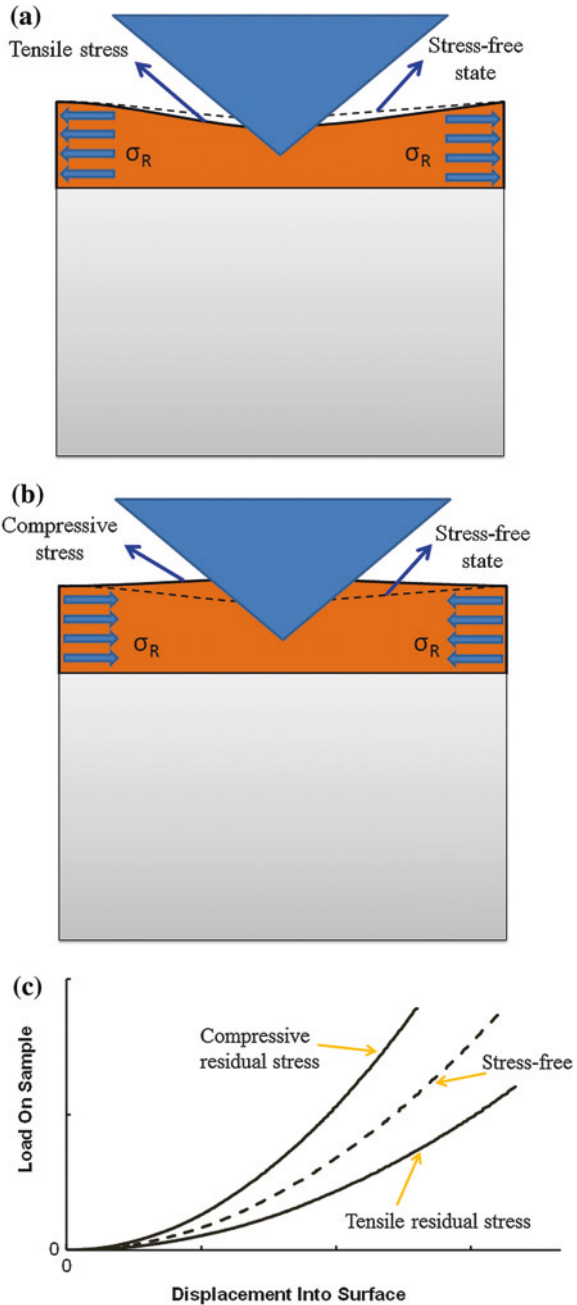
To solve this issue, it is proposed to use a focused ion beam (FIB) to produced stress-free micro-pillars on the specimen's surface (Fig. 2).

Fig. 2 Principle of ring-core drilling, and the idealized geometry of the remaining "stub"
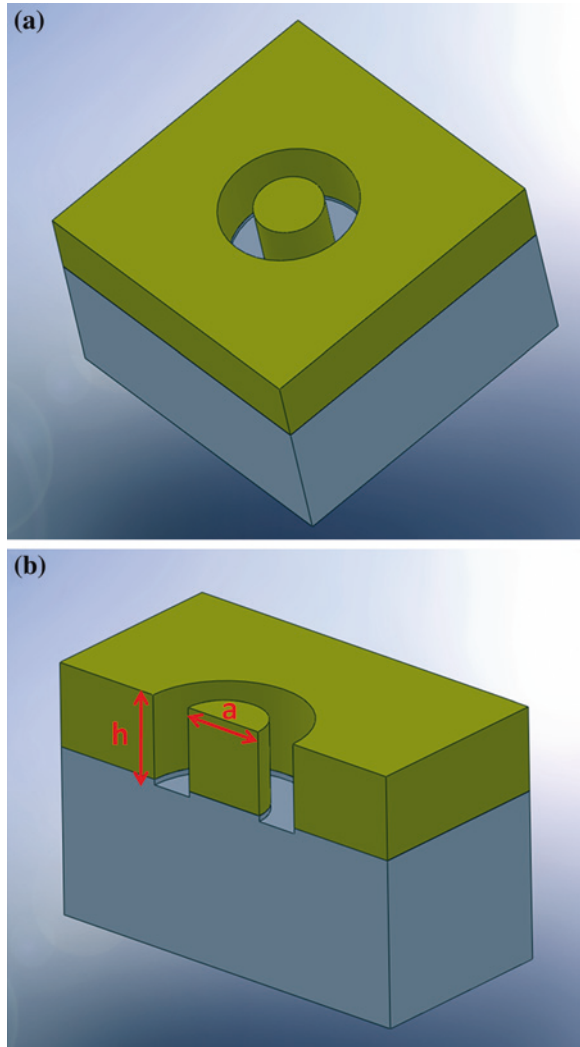

Recent publications by some of the authors (Korsunsky et al. 2009, 2010; Sebastiani et al. 2011; Song et al. 2012) showed that milling of annular trenches on a residually stressed surface gives full stress relaxation at specimen surface of the central stub for $h/a > 1$ (Fig. 1), thus allowing to obtain, for any kind of material and coating, a local stress-free reference volume (Korsunsky et al. 2010).

This result was obtained by Finite Element Modeling (FEM) of surface relaxation strain distribution after ring-core milling (Korsunsky et al. 2010).

The indentation on the stress relieved pillars gives the reference load–displacement data to be used for the application of the models and the evaluation of the

Fig. 3 Microstructure of the PVD TiN coating (columnar) on cemented carbide WC–Co substrate (Dye et al. 2001)
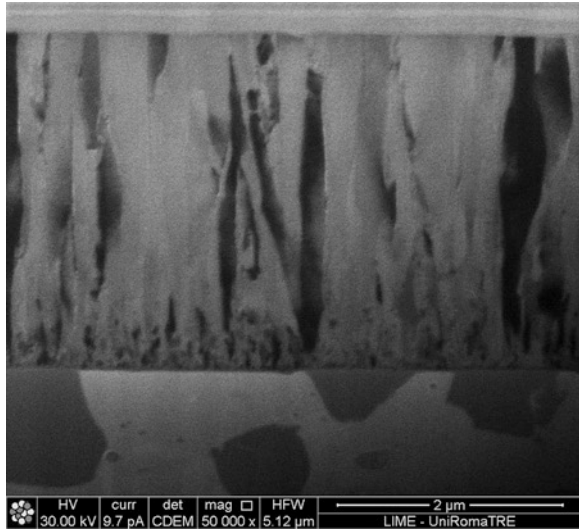
pristine residual stress by comparison with the load–displacement data on the residually stressed material.

The proposed methodology has been applied and validated in this work on a 3.8 μm CAE-PVD TiN coating on WC–Co substrate (see Fig. 3).

Most of the data reported in this book chapter were already presented in international conferences and published in the related conference proceedings (Sebastiani et al. 2010).

2 Models for the Analysis of Residual Stress by Instrumented Indentation and Effects on Fracture Behavior

Literature papers (Bemporad et al. 2008; Suresh and Giannakopoulos 1998; Tsui et al. 1996) have already demonstrated that the presence of a residual stress field at specimen surface can induce measurement inaccuracies in the conventional hardness and elastic modulus analysis procedures by nanoindentation.

Indeed, the influence of applied stress on hardness and apparent modulus was firstly analyzed by Tsui, Bolshakov and Pharr (Bolshakov et al. 1996; Tsui et al. 1996) by nanoindentation testing on 8009 Aluminum alloy and Finite Element Modeling.

These authors concluded that the observed influence of applied stress on measured hardness and modulus is actually due to changes in the real contact areas (measured by optical methods) as a function of the applied stress; in particular, higher compressive stress give higher real contact area, leading to an

overestimation of hardness and elastic modulus, as measured by the conventional Oliver-Pharr method(Oliver and Pharr 1992).

When the real contact areas are used for hardness and modulus calculation, they found that both the elastic modulus and hardness were independent of applied stress (Bolshakov et al. 1996; Tsui et al. 1996).

Therefore, sharp indentation testing can be used for the experimental evaluation of the average residual stress state at specimen surface (Suresh and Giannakopoulos 1998).

Several methods still exist in the literature for the evaluation of residual stress and strain by sharp indentation testing, all mainly based on the comparison between the load-depth curve obtained on a residually stressed surface with the corresponding results on the stress-free (or virgin) reference material (Suresh and Giannakopoulos 1998).

Suresh and Giannakopoulos (Suresh and Giannakopoulos 1998) presented a general methodology for the determination of surface (equi-biaxial) elastic residual stress by instrumented sharp indentation testing, based on the original observations made by Pharr's group (Bolshakov et al. 1996; Tsui et al. 1996).

This methodology (Suresh and Giannakopoulos 1998) is based on the main assumption that the average contact pressure due to indentation is unaffected by any preexisting elastic residual stress (invariance of indentation hardness).

A detailed explanation of why the real hardness cannot be affected by any biaxial residual stress is given in detail in the Suresh and Giannakopoulos paper (Suresh and Giannakopoulos 1998).

The concept of this method is depicted in Fig. 1. The principle is that a biaxial residual stress will involve a modification of the contact area during indentation, leading to either a more pronounced sinking-in (Fig. 1a) in case of tensile residual stress or a more a piling-up (Fig. 1b) in case of compressive residual stress, in comparison to the contact area corresponding the stress-free state.

The corresponding modifications of the load displacement curve in comparison to the stress-free state are reported in Fig. 1c.

Basing on this principle, a general relationship between the ratio of contact areas at a fixed depth between the stressed surface and the stress-free (virgin) reference material (or equivalently the ratio of penetration depths at a fixed load) was then given (Fischer et al. 2005):

$$\frac{A}{A_0} = \left(1 + \frac{\sigma_{res}}{H_0}\right)^{-1} \tag{1}$$

$$\frac{h^2}{h_0^2} = \left(1 - \frac{\sigma_{res}}{H_0}\right)^{-1} \tag{2}$$

where σ_{res} is the average biaxial residual stress (negative value if compressive), H_0 is the average contact pressure due to indentation (i.e. the hardness), (A_0, h_0) and

(A, h) are the real contact area and penetration depth for the stress free reference material and the stressed material, respectively.

The proposed methods were successfully applied (Suresh and Giannakopoulos 1998) on artificially strained samples, where the reference curve for the stress-free material is easily measurable and external controlled stress states can be simply applied.

Nevertheless, strong limitations still exist when such methods are applied for the analysis of real residual stress states on polycrystalline materials and thin coatings, essentially due to the fact that a reference load-depth curve for the unstressed material is often not available (or achievable after complex sample preparation procedures), especially in case of nanostructured materials and thin films.

In the methodology proposed here, the existing limits of the available methods for stress calculation from sharp indentation testing are overcome by introducing an original methodology for the local residual stress relieving over a stressed surface.

A complete relief of residual stress is induced by FIB milling of annular trenches at specimen surface, if the depth of the milled trenches are higher than their characteristic diameter (Korsunsky et al. 2010).

Nanoindentation testing over stress relieved stubs then gives the stress-free reference load-depth curve to be used for residual stress calculation by Eqs. (1) and (2) (Suresh and Giannakopoulos 1998).

The additional boundary conditions given by the presence of the edges of pillar and by coating/substrate interface can also be considered during the stress calculation by analytical modeling of contact stresses, Film Doctor® software, as described in the next chapter.

In addition to this, nanoindentation testing over the stress relieved pillars also allows (1) a more proper evaluation of hardness and modulus of the coating by using the conventional Oliver-Pharr method and (2) to analyze the effects of residual stress on fracture toughness of the coating.

To evaluate this latter effect (Anstis et al. 1981; Toonder et al. 2002), nanoindentation under load-controlled conditions is performed on pillar structures, up to a maximum load where a controlled fracture of the pillar can be induced.

Fracture toughness can be then evaluated by the measurement of the dissipated energy by brittle fracture through the coating during nanoindentation testing (Chen and Bull 2009; Toonder et al. 2002).

According to the model proposed by Toonder et al. (2002), a through thickness cracking during sharp instrumented indentation will cause a drop in the measured displacement, in case of load-controlled nanoindentation.

(1) Lower and (2) upper bounds for the dissipated energy U_{fr} can be obtained by direct measurement on the load-depth curve in correspondence of the failure, by assuming that material's behavior is either (1) fully elastic or (2) fully plastic before and after cracking (Chen and Bull 2009).

Fracture toughness can be therefore evaluated by the following equation:

$$K_C = \left[\frac{E_f \cdot U_{fr}}{(1 - \nu^2) \cdot A_{crack}} \right]^{\frac{1}{2}} \tag{3}$$

where A_{crack} is the actual surface of crack in the coating (Toonder et al. 2002), which is often measured directly by optical or SEM microscopy observations of the cracks.

Obviously, indentation on pillars gives the fracture toughness of the stress-free material.

Consequently, the actual toughness of the residually stressed coating can be evaluated by the following equation, which takes into account the influence of residual stress on fracture toughness:

$$K_C = K_C^0 + Z \cdot \sigma_R \cdot c^{1/2} \tag{4}$$

where σ_R is the average surface residual stress, c is the radial dimension of the crack and Z is a crack-geometry parameter, which is equal to 1.26 when the radial dimension of the crack is equal to its depth.

3 Software Assisted Correction for Substrate/Edge Effects and Residual Stress Calculation by the Use of Analytical Modeling (Film Doctor®)

The models for residual stress analysis by indentation that were presented in the previous chapter are based on the geometrical boundary conditions of a homogeneous half-space being indented by an axisymmetric indenter.

Conversely, the experimental methodology that is being presented here consists of the indentation on micro-pillars realized on a coating-substrate system.

In order to assess the validity of those models in the present case, it is necessary to take into account (1) the layered character of the system under examination and (2) the effect of edges (Jakes et al. 2009) in case of indentation on pillar structure; this means two additional boundary conditions that could affect the results of residual stress calculation.

A commercial software package FilmDoctor® (FilmDoctor® 2013; Schwarzer et al. 2001) was adopted for the analytical modeling of the experimentally measured unloading curves for the cases of (1) residually stressed coating and (2) stress relieved coating.

The adopted software evaluates the complete elastic stress field in the moment of beginning unloading by the use of an Extended Hertzian Theory (FilmDoctor® 2013; Schwarzer et al. 2001), and allows to consider the additional boundary conditions given by (1) substrate and edges and (2) to include the presence of residual stress.

The final procedure for residual stress analysis can be summarized as follows:

- **Step-1:** Determination of the correct coating Elastic modulus by analyzing the experimental unloading curves obtained on stress relieved pillar structures.
- **Step-2:** Determination of the true coating yield strength by analyzing the experimental unloading curves obtained on stress relieved pillar structures, after

evaluation of the von Mises stress in the moment of beginning unloading from the unloading curve of the pillars.

- **Step-3:** Determination of the apparent coating yield strength by analyzing the unloading curves obtained on the stressed (undisturbed) coating, after evaluation of the von Mises stress in the moment of beginning unloading from the unloading curve of the half space (no pillar). This gives apparent higher coating yield strength (in the case of compressive residual stress) because the high intrinsic stresses also explain higher hardness and thus, lower indentation depth at same load in comparison with pillar structure.
- **Step-4:** Determination of the intrinsic stress by fitting the biaxial stress to the true yield strength for same loading situation as given in step 3; evaluation of the von Mises stress in the moment of beginning unloading from the unloading curve of the half space but now with biaxial intrinsic stress taken into account. Fitting the biaxial stress to the true yield strength from step 2. In order to obtain a quantitative estimation of the effect of adopted corrections for edge and substrate effects, residual stresses were also calculated by Eqs. (1–2) at several penetration depths, performing also a quantitative evaluation of the critical penetration depth, below which the edge effects are not relevant anymore.

4 Experimental Details

The experimental activities were focused on a 3.8 µm TiN coating deposited on a WC–Co substrate by CAE-PVD using the following deposition parameters (also reported in (Bemporad et al. 2007)): pressure 1.5 Pa, deposition temperature 450 °C, applied bias voltage 150 V, current 70 A. The coating and substrate microstructures are illustrated in Fig. 3.

Annular FIB milling was performed using FEI Helios Nanolab 600 DualBeam FIB/SEM equipment, using current of 48 pA at 30 kV and adopting outer-to-inner path of the ion beam to reduce re-deposition over the island surface. A series of regular cross sections was also realized before ring milling in proximity of the pillar volume in order to minimize re-deposition over the pillar surface. The beam drift was also monitored during milling and correction applied as necessary.

Based on the FEM results reported in a previous work by some of the authors (Korsunsky et al. 2010), the maximum milling depth and the outer diameter of the island were fixed at 3.8 µm (equal to the coating thickness) to ensure that complete strain relief was achieved.

A complete dimensional characterization of each produced pillar (surface diameter, overall depth, lateral slope) was also performed by high resolution in situ SEM imaging.

Fifteen pillars were realized over a surface area of about 0.2×0.2 mm^2.

Indentation testing was then performed on both pillar structures and undisturbed (residually stressed) surface by a Nano Indenter G200 (Agilent technologies), with a Berkovich indenter calibrated on certified fused silica reference sample.

Indentations on pillar structures (ten tests) were performed in a continuous stiffness measurement (CSM) mode, under a constant strain rate of 0.05 s^{-1}. A maximum penetration depth of 200 nm was set for all tests, in order to avoid cracking of the stress relieved pillars during indentation and to minimize the edge and substrate effects.

The actual shapes of the residual indents were in all cases analyzed by SEM-FEG analysis. The real contact area in both cases of stress relieved pillars and undisturbed surface was also numerically estimated by image analysis on high resolution SEM micrographs; hardness and elastic modulus were consequently re-calculated.

Deformation mechanisms of the TiN coating under normal indentation were investigated as a function of the applied load by FIB-TEM techniques.

A lamella for TEM observation was also prepared by FIB technologies in correspondence of a high load (5 N) Vickers indentation: microstructural observations were performed both by in situ SEM after FIB sectioning and by TEM-SAED analysis. In this latter case, the influence of substrate plastic deformation on the deformation mechanisms of the coating was also investigated.

As reported in the following of this paper, a strong tendency to brittle failure was observed in the stress relieved pillars, while no cracking was observed in the residually stressed coating even for relatively high applied load (up to 500 mN). This suggested that residual stress can play a crucial role in determining the cracking behavior of the TiN coating under investigation.

Therefore, five more tests were performed on pillar structures under load controlled conditions. A maximum applied load of 30 mN was set, in order to have radial cracking of the TiN coating without any further damaging of the Pillar.

Fracture toughness was analyzed by the Toonder bound model (Toonder et al. 2002), which was briefly described in the previous chapter of this paper.

The average residual stress inside the coating was finally independently measured by a Dmax-RAPID Rigaku micro-diffractometer equipped with a cylindrical image plate (IP) detector and a collimator diameter of 300 µm, using Cu-Kα radiation. Average residual stresses were calculated by the analysis of a single Debye ring via the conventional d versus sin$^2\psi$ plot (Gelfi et al. 2004). The depth of the X-ray gauge volume used in this case corresponded to the coating thickness.

5 Results

The summary of obtained results is reported in the Table 1. An SEM micrograph of some of the FIB-produced pillars is presented in Fig. 4a–b: it is worth noting that no surface modification are induced on the pillar surface by the FIB milling and that the actual shape of the pillar (dimensions, slope of the lateral walls) is essentially identical to the ideal one used for modeling and stress calculations (lateral slope lower than 2°, Fig. 3c).

Figure 3d shows pillars with Berkovich indentation at their center, as indicated by arrows; the average off-center of indentation was of the order of 0.4 µm (which is in any case lower than the nominal positional accuracy of the nanoindenter, which is 1 µm).
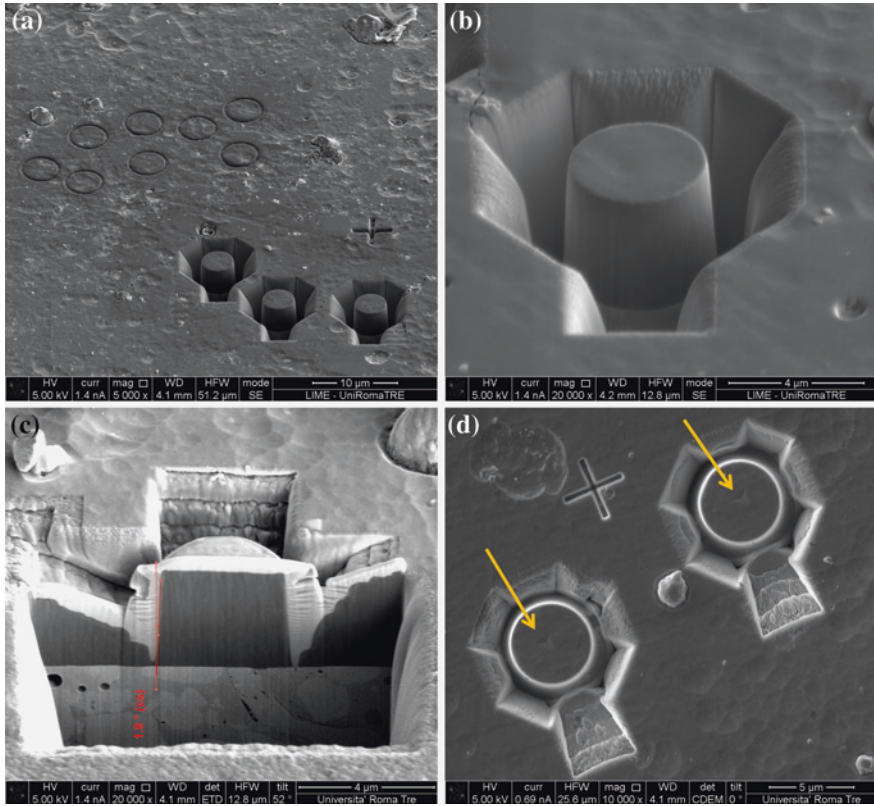
Fig. 4 **a** Example of some of the realized pillar structures before indentation and **b** detail of one of the pillars; **c** FIB/SEM cross section observation of one of the pillar; **d** pillars after indentation (Berkovich indentation can be seen at pillar's centers)

Table 1 *Left column*: apparent properties of the TiN coating under investigation as measured by conventional nanoindentation on the undisturbed surface and *Right column*: real properties (including residual stress and fracture toughness) after indentation testing on stress relieved pillars and the application of the new proposed methodology

	Apparent properties of the TiN coating as measured by conventional nanoindentation	Real properties as evaluated after nanoindentation testing on stress relieved pillars and modeling
E (GPa)	543.00 ± 23.35	500.17 ± 21.34
H (GPa)	31.88 ± 2.80	27.05 ± 2.80
σ_{res} (GPa)	–	-5.63 ± 0.85
K_{IC} (mPa·m$^{0.5}$)	–	$6.09 \leq K_C \leq 7.46$
K_{IC} including σ_{res} (mPa·m$^{0.5}$)	–	$19.54 \leq K_{C(with\ stress)} \leq 20.91$

Fig. 5 **a** set of load displacement cures on the residually stressed TiN coating; **b** comparison between the load–displacement curves obtained on the stressed surface and the stress relieved pillars; **c** full data set for indentation on pillars
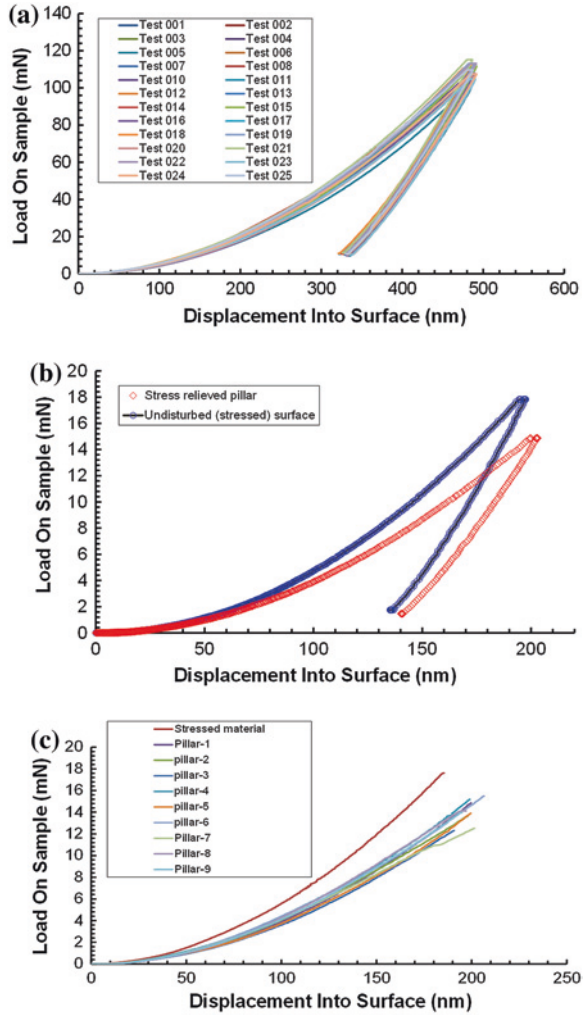
The results for nanoindentation on the undisturbed (residually stressed) coating are presented in Fig. 5a, while a comparison between load-depth curves obtained on the stressed surface and on stress relieved pillars is then reported in Fig. 5b: this results clearly show that strong compressive residual stresses are present in the TiN coating under examination. Figure 5c also shows a good repeatability over nine different measurements on the pillar structures.

On the basis of nine repeated tests carried out in this study, the average value of residual stress in the coating, obtained with the stress calculation procedure reported in the previous chapter (substrate and edge effect on indentation behavior taken into account), was found to be equal to -5.63 ± 0.85 GPa, as also reported
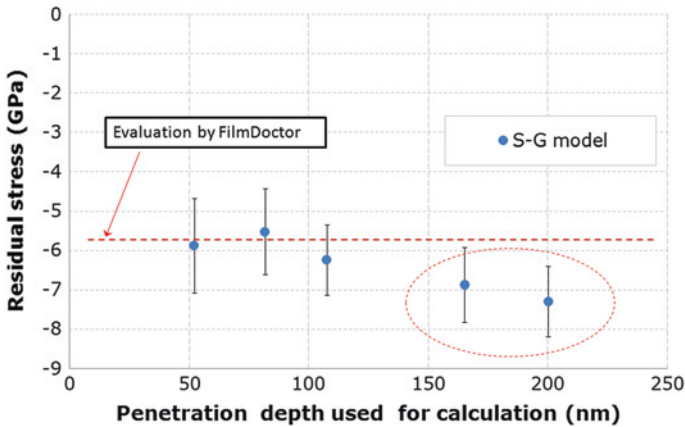
Fig. 6 Stress calculation by the Suresh-Giannakopoulos model (Suresh and Giannakopoulos 1998) at different penetration depths (Eq. 2) and comparison (*dashed line*) with results obtained by FilmDoctor® (Schwarzer et al. 2001)

in Table 1 and highlighted by a dashed line in Fig. 6. The results for contact stress distribution obtained by film doctor are reported in the Fig. 7.

The obtained residual stress value is in good agreement with the estimate obtained by XRD analysis of −5.84 GPa (Korsunsky et al. 2010), although XRD data analysis contained a greater uncertainty due to the strong texture of the TiN coating.

Figure 6 also reports results of stress calculations by the conventional Suresh-Giannakopoulos (S-G) model (Suresh and Giannakopoulos 1998) in comparison with the stress value obtained by FilmDoctor® analysis: it is evident that close agreement is found between the two methods when the stress calculation with the S-G model is performed for penetration depths lower than 120 nm, while for higher penetration depths some discrepancies between the two methods are found (at maximum penetration depth a value of −7.4 GPa is calculated by the S-G model).

This is most probably due to the influence of both the edges and the substrate (not considered in the S-G model) which involve an overestimation of the compressive residual stress for a relative penetration depth higher than 1/30 of the pillar diameter, that can be assumed as the critical penetration depth (for this particular coating/substrate combination), below which the effects of edges and substrate are not relevant anymore.

Figure 8(a–d) show the FEG-SEM micrographs of the indentation marks performed on (a–b) undisturbed (residually stressed) coating and (c–d) stress relieved pillar: a strong difference between the actual indent morphology is clearly visible.

In particular, the occurrence of piling-up due to compressive stress (as observed in previous works (Bolshakov et al. 1996; Tsui et al. 1996) is evident for the residually stressed surface, as clearly visible in Fig. 8a and in the FIB cross-section of an indentation mark reported in Fig. 8e.
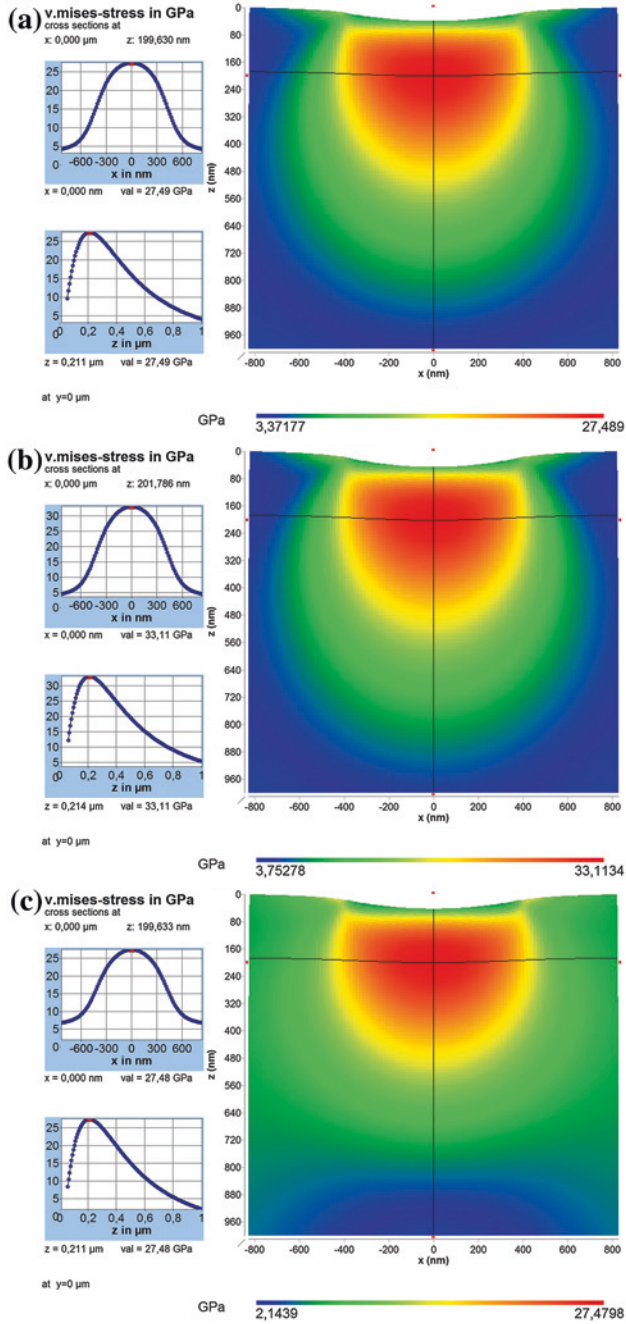
Fig. 7 a Example of modeling by Filmdoctor® (Schwarzer et al. 2001): True Yield strength of coating material with Y = 27.461 GPa, **b** apparent higher yield strength of stressed coating with 33.111 GPa and **c** true yield strength of stressed coating by taking the biaxial intrinsic stress of −5.6 GPa into account
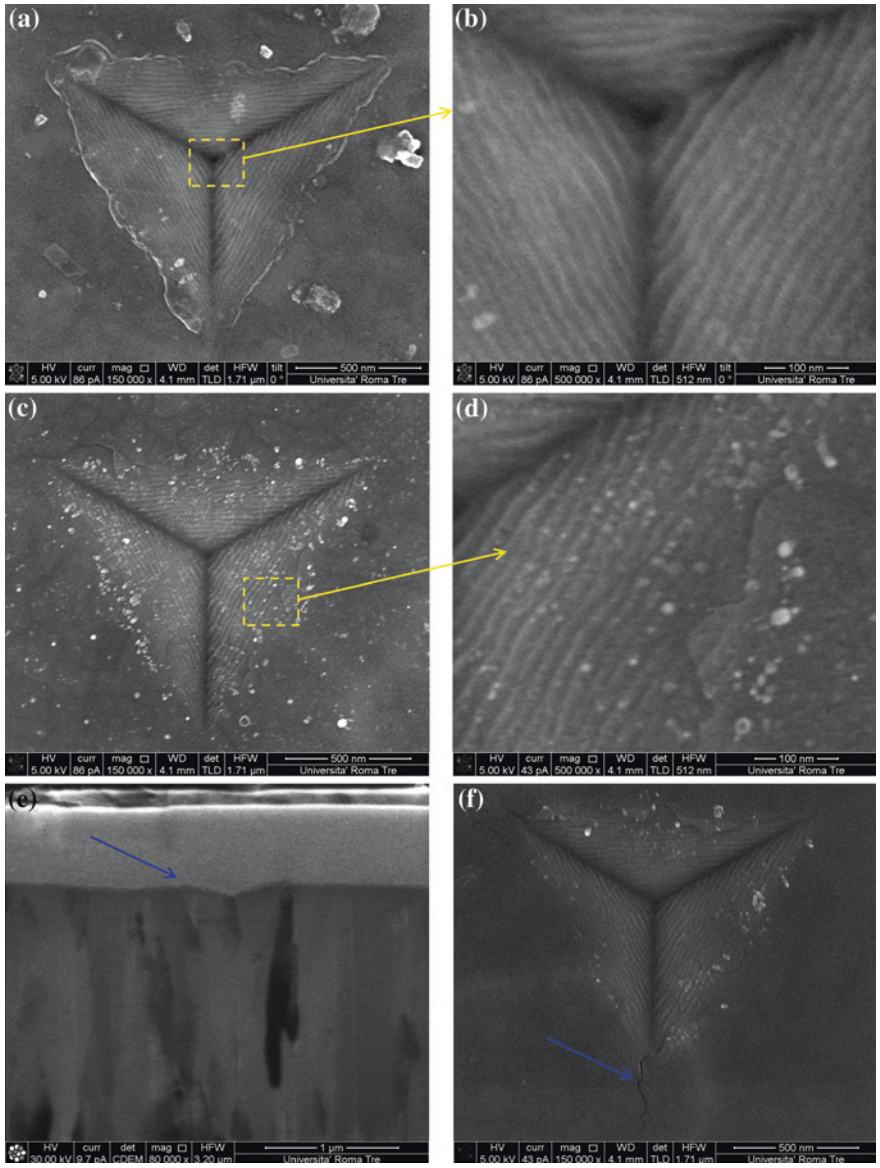
Fig. 8 SEM-FEG observation of produced indentation marks on (**a–b**) undisturbed (stressed) surface and (**c–d**) pillar structure; (**e**) FIB cross-section in correspondence of one indentation and (**f**) evidence of cracks during indentation on the stress-relieved pillars

SEM-FEG analyses also allowed to do a quantitative evaluation of contact area and perform a re-evaluation of coating's hardness and elastic modulus, which were significantly over-estimated (due to piling-up) when calculated by the conventional Oliver-Pharr method after nanoindentation on the undisturbed surface (see Table 1).

For the indentations reported in Fig. 8a–d, the measured contact areas were of 8.98·10^3 nm^3 for indentation on the virgin material (Fig. 8a) and 6.55·10^3 nm^3 for the stress relieved pillar (Fig. 8d). When the actual contact area is known, residual stress can also be calculated from the Eq. (2). In this case, the value of −7.30 GPa was calculated, which is close to the average value of −7.4 GPa calculated by the Eq. (1) at maximum penetration depth (Fig. 6).

It is worth noting that after re-evaluation of contact areas by SEM observation, the hardness and elastic modulus measured on the undisturbed (stressed) surface were very similar to the ones obtained on the stress relieved pillars, thus confirming that hardness and elastic modulus are essentially independent of surface elastic residual stress (Suresh and Giannakopoulos 1998).

The FEG-SEM micrographs of the indentations performed on both pillar structure and stressed surface (details showed in Figs. 8b, d) clearly show that plastic deformation at the nano-scale essentially occurs by formation of nano-shear bands (average size 15 nm) inside the columnar grains with no reciprocal sliding of the grain boundaries, independently of the presence of residual stress.

On the other hand, a complete modification of the deformation mechanisms has been observed in case high load Vickers indentation testing: observing the FIB/SEM cross section analysis reported in Fig. 9.

In particular, TEM-SAED analysis confirmed that deformation mechanisms essentially consist of (1) grain boundary cracking and reciprocal sliding when deforming over the Cobalt matrix (Fig. 9b) and (2) complete grain deformation, recrystallization (see SAED pattern in Fig. 9c) and interface delamination over the (harder) WC-grains.

It is therefore clear that deformation mechanisms at high load are essentially driven by the mechanical properties of the substrate (Fig. 9a).

Conversely, strong influence of residual stress on the fracture behavior of the coating was observed.

Figure 10 shows one the indentations load-depth curves realized under load-controlled conditions for fracture toughness analysis (Anstis et al. 1981; Chen and Bull 2009), and the observation of a broken pillar after testing.

The horizontal drop of the displacement during indentation indicates the complete brittle failure of the coating.

Figure 10b also show that failure of the pillar essentially occurs by brittle failure into three identical segments, following the three-side geometry of the Berkovich indenter: this observation allows the estimation of the actual area of fracture to be used in Eq. (3) for fracture toughness calculation, which is (under the assumption of smooth surface, see Fig. 2b for symbols):

$$A_{fr} = k \cdot 3 \cdot \left(\frac{a}{2} \cdot h \right) \tag{5}$$

where k is a correcting factor (always ≥ 1) which takes into account that the fracture surfaces are not smooth at all.

In this case, fracture surfaces appear to be very irregular, due to the fact that it propagates along the grain boundaries of the coating: it is therefore likely that the actual area of fracture is higher than the ideal one ($k > 1$ in Eq. (5)): an estimated
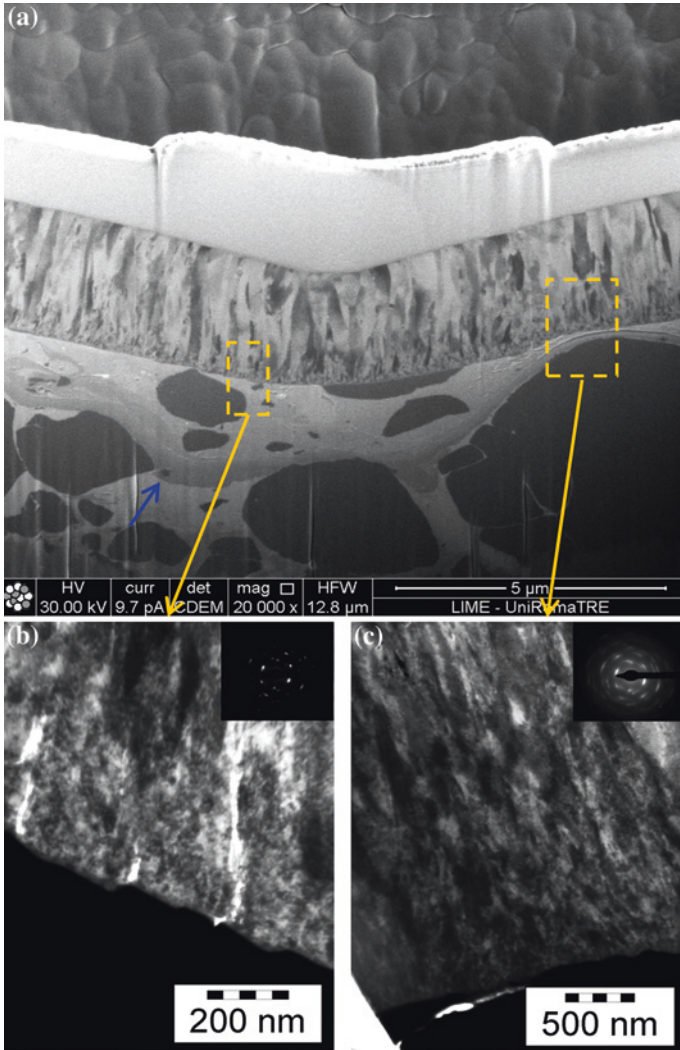
Fig. 9 a FIB/SEM observation of the cross section of a Vickers indentation mark (5 N) show-ing severe plastic deformation of the Cobalt matrix in the substrate, **b–c** TEM observation of deformation mechanisms in different areas of the coating. In this case, deformation mechanisms essentially depend on the mechanical behavior of the substrate

value of $k = 2$ (which is likely in case of fracture propagation along a (100) direc-tion) was therefore taken for toughness calculation.

Fracture toughness of the (stress relieved) TiN coating was then calculated by the use of the Toonder et al. bound model (Eq. (3), (Toonder et al. 2002)) as:

$$6.09 \leq K_C \leq 7.46 \left(\mathrm{MPa} \cdot \mathrm{m}^{0.5} \right) \tag{5}$$

Fig. 10 Measurement of fracture toughness by load-controlled nanoindentation on pillars. **a** example of a load-depth curve showing the brittle failure of the pillar and **b** SEM observation of one of the broken pillars, revealing fracture morphology to be used for toughness calculation [34]
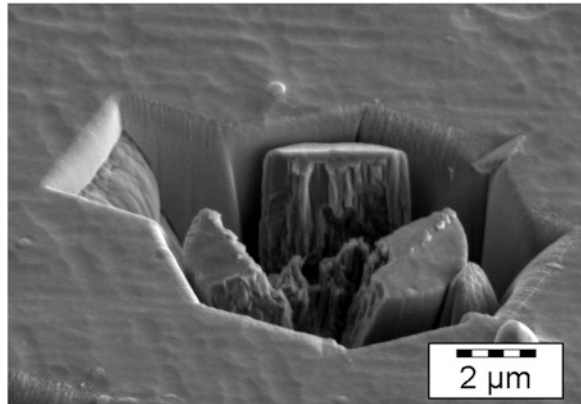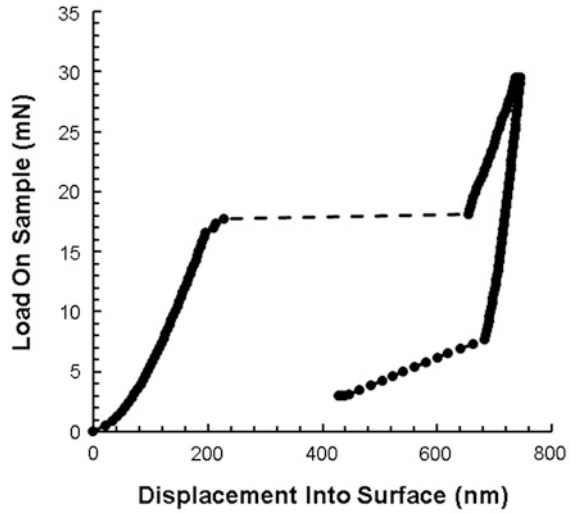
In addition, the influence of residual stress on fracture toughness was evaluated by the use of Eq. (4) (Anstis et al. 1981): in this case, the presence of a compressive stress of −5.63 GPa leads to a fracture toughness (stress dependent) of the coating of:

$$19.54 \leq K_{C(with\,stress)} \leq 20.91 \left(MPa \cdot m^{0.5}\right) \tag{6}$$

This explains why no cracking under sharp indentation is usually observed on highly stressed hard PVD coatings, even under very high applied normal load.

A summary of mechanical characterization activities is reported in Table 1, where the effect of residual stress on the nano-mechanical characterization of the coating can be evaluated by the comparison between different results obtained on stress relieved pillars and undisturbed surface.

6 Discussion

In this work, an optimized procedure for the analysis of residual stress effects on the nano-mechanical behavior of thin coatings is presented, based on the integrated adoption of FIB milling and nanoindentation testing.

The methodology allows for the quantitative evaluation of the surface elastic residual stress on a micron scale, by using well-established experimental techniques that can be easily reproduced on FIB equipments (Bei et al. 2007; Uchic et al. 2004).

The application on a PVD TiN coating showed a good agreement between the new method and the estimation obtained by the conventional XRD $\sin^2 \psi$ method.

It is important to remind that only the in-plane average stress can be evaluated by this procedure: nonetheless, residual stresses are usually assumed as equi-biaxial in case of thin coatings (Chason et al. 2002; Davis 1993; Detor et al. 2009; Marks et al. 1996; Pao et al. 2007; Uchic et al. 2004; Windischmann 1987), so the proposed method can be a reliable way for stress analysis in this specific case.

At this point, some more considerations are necessary on the adopted assumption during stress calculation. The adoption of Eqs. (1–2) is based on the assumptions that (1) the elastic behavior of the analyzed coating is homogeneous and isotropic and (2) that continuum mechanics is still valid at the considered scale.

An SEM micrograph of the TiN coating is reported in Fig. 3, where a strong columnar microstructure is evident: this indicates that some inaccuracies in stress calculation could arise as a consequence of a not proper estimation of the actual elastic anisotropy of the coating.

However, the observed deformation mechanisms at the nanoscale (Fig. 8) show that grain boundaries are not involved in the deformation mechanisms for penetration depths below 200 nm.

Therefore, the assumption of isotropic elastic behavior of the coating could be a reasonably choice, at least at the considered scale, where grain boundaries are not involved in the deformation mechanisms.

Anyway, the use of similar elastic constant and a similar probing volume guarantee the consistency between residual stress values measured by the XRD-sin2ψ and nanoindentation method.

It is also important to comment on standard deviation of the calculated residual stress, that was about 0.85 GPa: such variation of experimentally measured values is likely due also to a real variation of residual stress from point to point, probably due to the non-homogeneity of the WC–Co substrate (see Fig. 3). This effect is surely superimposed to the uncertainty of the method itself and further work is now ongoing on simpler systems in order to clarify this point.

Table 1 reports a comparison between the apparent properties as measured by conventional analysis of nanoindentation data obtained on the stressed surface and the actual properties (including residual stress and toughness) as measured by indentation on stress relieved pillars.

The obtained results on fracture toughness show that residual stress plays a significant role in determining the "in-service" toughness of the PVD coating

(including stress) applied to a specific substrate. As a consequence, toughness data without knowing the real residual stress of the specific sample cannot give afford-able values to be used in different context, nor this information can be used in different systems (i.e. different substrate, even if with a coating obtained with the same deposition process and parameters).

On the other hand, indentation testing on stress relieved pillars also gives the "stress-free fracture toughness" of the coating (i.e. without the effect of residual stress) giving an unbiased value to better predict the in-service fracture behavior of the coatings when external forces (i.e. contact load) will be applied.

It is also worth noting that the application of the Toonder et al. (Toonder et al. 2002) bound model revealed to be particularly effective when applied to the well confined geometry which characterizes the stress relieved pillars.

In fact, in case of indentation of pillars the geometry of the cracks is very well defined and can be evaluated by SEM observation after testing; a more accurate evaluation of fracture toughness can be therefore performed, in comparison with the conventional procedure (which requires radial chipping of the coating).

In addition, it is also important to remind that in case of strong compressive stress (e.g. the TiN coating under investigation), the measurement of fracture toughness by sharp indentation on the undisturbed surface is often not possible at all, simply because residual stresses inhibit any radial cracking, even at very high applied load.

The proposed methodology gives then a more complete framework of the effect of residual stress on the nano-mechanical and fracture behavior of thin coatings and can be a robust support for a more proper prediction of in-service mechanical behavior and failure modes.

7 Concluding Remarks

In this work, a new methodology for residual stress measurement in thin films and small scale systems is presented, based on nanoindentation testing on FIB-produced pillars.

First results of stress measurement on a TiN hard coating reported in this paper are promising, and a good agreement was found with the estimation obtained by XRD $\sin^2\psi$ analysis.

The new method gives a statistically reliable, robust and very site-specific eval-uation of the surface residual stress field, giving also further information on the effect of residual stress on nano-mechanical behavior of hard coatings.

In fact, the proposed procedure also allows a more correct evaluation of other key-properties, such as hardness and modulus (which are usually affected by sig-nificant measurement errors due to the presence of residual stress) and fracture toughness as a function of the residual stress state.

References

Anstis GR, Chantikul P, Lawn BR, Marshall DB (1981) A critical evaluation of indentation techniques for measuring fracture toughness: i, direct crack measurements. J Am Ceram Soc 64(9):533–538. doi:10.1111/j.1151-2916.1981.tb10320.x

Bei H, Shim S, Miller MK, Pharr GM, George EP (2007) Effects of focused ion beam milling on the nanomechanical behavior of a molybdenum-alloy single crystal. Appl Phys Lett 91(11):111915

Bemporad E, Sebastiani M, Casadei F, Carassiti F (2007) Modelling, production and characterisation of duplex coatings (HVOF and PVD) on Ti–6Al–4 V substrate for specific mechanical applications. Surf Coat Technol 201(18):7652–7662. doi:http://dx.doi.org/10.1016/j.surfcoat.2007.02.041

Bemporad E, Sebastiani M, Staia MH, Puchi Cabrera E (2008) Tribological studies on PVD/HVOF duplex coatings on Ti6Al4 V substrate. Surf Coat Technol 203(5–7):566–571. doi:http://dx.doi.org/10.1016/j.surfcoat.2008.06.055

Bolshakov A, Oliver WC, Pharr GM (1996) Influences of stress on the measurement of mechanical properties using nanoindentation: Part II. Finite element simulations. J Mater Res 11(03):760–768. doi:10.1557/JMR.1996.0092

Bull SJ (2005) Nanoindentation of coatings. J Phys D Appl Phys 38(24):R393

Bull SJ, Berasetegui EG (2006) An overview of the potential of quantitative coating adhesion measurement by scratch testing. Tribol Int 39(2):99–114. doi:http://dx.doi.org/10.1016/j.triboint.2005.04.013

Chason E, Sheldon BW, Freund LB, Floro JA, Hearne SJ (2002) Origin of compressive residual stress in polycrystalline thin films. Phys Rev Lett 88(15):156103

Chen J, Bull SJ (2009) Modelling the limits of coating toughness in brittle coated systems. Thin Solid Films 517(9):2945–2952. doi:http://dx.doi.org/10.1016/j.tsf.2008.12.054

Davis CA (1993) A simple model for the formation of compressive stress in thin films by ion bombardment. Thin Solid Films 226 (1):30-34. doi:http://dx.doi.org/10.1016/0040-6090(93)90201-Y

Detor AJ, Hodge AM, Chason E, Wang Y, Xu H, Conyers M, Nikroo A, Hamza A (2009) Stress and microstructure evolution in thick sputtered films. Acta Materialia 57(7):2055–2065. doi:http://dx.doi.org/10.1016/j.actamat.2008.12.042

Dye D, Stone HJ, Reed RC (2001) Intergranular and interphase microstresses. Curr Opin Solid State Mater Sci 5(1):31–37. doi:http://dx.doi.org/10.1016/S1359-0286(00)00019-X

Espinosa HD, Prorok BC, Fischer M (2003) A methodology for determining mechanical properties of freestanding thin films and MEMS materials. J Mech Phys Solids 51(1):47–67

FilmDoctor® (2013) software for the evaluation of mechanical contact for homogeneous and layered materials. www.siomec.de/FilmDoctor. 2013

Fischer W, Malzbender J, Blass G, Steinbrech RW (2005) Residual stresses in planar solid oxide fuel cells. J Power Sources 150:73–77. doi:http://dx.doi.org/10.1016/j.jpowsour.2005.02.014

Gelfi M, Bontempi E, Roberti R, Depero LE (2004) X-ray diffraction Debye Ring Analysis for STress measurement (DRAST): a new method to evaluate residual stresses. Acta Materialia 52(3):583–589. doi:http://dx.doi.org/10.1016/j.actamat.2003.09.041

Jakes JE, Frihart CR, Beecher JF, Moon RJ, Resto PJ, Melgarejo ZH, Suárez OM, Baumgart H, Elmustafa AA, Stone DS (2009) Nanoindentation near the edge. J Mater Res 24(03):1016–1031. doi:10.1557/jmr.2009.0076

Korsunsky AM (2009) Eigenstrain analysis of residual strains and stresses. J Strain Anal Eng Des 44(1):29–43. doi:10.1243/03093247jsa423

Korsunsky AM, Sebastiani M, Bemporad E (2009) Focused ion beam ring drilling for residual stress evaluation. Mater Lett 63(22):1961–1963. doi:http://dx.doi.org/10.1016/j.matlet.2009.06.020

Korsunsky AM, Sebastiani M, Bemporad E (2010) Residual stress evaluation at the micrometer scale: Analysis of thin coatings by FIB milling and digital image correlation. Surf Coat Technol 205(7):2393-2403. doi:http://dx.doi.org/10.1016/j.surfcoat.2010.09.033

Marks NA, McKenzie DR, Pailthorpe BA (1996) Molecular-dynamics study of compressive stress generation. Phys Rev B 53(7):4117–4124

Oliver WC, Pharr GM (1992) An improved technique for determining hardness and elastic modulus using load and displacement sensing indentation experiments. J Mater Res 7(06):1564–1583. doi:10.1557/JMR.1992.1564

Oliver WC, Pharr GM (2004) Measurement of hardness and elastic modulus by instrumented indentation: advances in understanding and refinements to methodology. J Mater Res 19(01):3–20. doi:10.1557/jmr.2004.19.1.3

Pao C-W, Foiles SM, Webb EB III, Srolovitz DJ, Floro JA (2007) Thin film compressive stresses due to adatom insertion into grain boundaries. Phys Rev Lett 99(3):036102

Pauleau Y (2001) Generation and evolution of residual stresses in physical vapour-deposited thin films. Vacuum 61(2–4):175–181. doi:http://dx.doi.org/10.1016/S0042-207X(00)00475-9

Roy RK, Lee K-R (2007) Biomedical applications of diamond-like carbon coatings: A review. J Biomed Mater Res B Appl Biomater 83B(1):72–84. doi:10.1002/jbm.b.30768

Schwarzer N, Hermann I, Chudoba T, Richter F (2001) Contact modelling in the vicinity of an edge. Surf Coat Technol 146–147:371–377. doi:http://dx.doi.org/10.1016/S0257-8972(01)01418-9

Sebastiani M, Bemporad E, Carassiti F, Schwarzer N (2010) Residual stress measurement at the micrometer scale: focused ion beam (FIB) milling and nanoindentation testing. Phil Mag 91(7–9):1121–1136. doi:10.1080/14786431003800883

Sebastiani M, Eberl C, Bemporad E, Pharr GM (2011) Depth-resolved residual stress analysis of thin coatings by a new FIB–DIC method. Mater Sci Eng: A 528(27):7901–7908. doi:http://dx.doi.org/10.1016/j.msea.2011.07.001

Song X, Yeap KB, Zhu J, Belnoue J, Sebastiani M, Bemporad E, Zeng K, Korsunsky AM (2012) Residual stress measurement in thin films at sub-micron scale using Focused Ion Beam milling and imaging. Thin Solid Films 520(6):2073–2076. doi:http://dx.doi.org/10.1016/j.tsf.2011.10.211

Suresh S, Giannakopoulos AE (1998) A new method for estimating residual stresses by instrumented sharp indentation. Acta Materialia 46(16):5755–5767. doi:http://dx.doi.org/10.1016/S1359-6454(98)00226-2

Teixeira V (2002) Residual stress and cracking in thin PVD coatings. Vacuum 64(3–4):393–399. doi:http://dx.doi.org/10.1016/S0042-207X(01)00327-X

Toonder JD, Malzbender J, With GD, Balkenende R (2002) Fracture Toughness and Adhesion Energy of Sol-gel Coatings on Glass. J Mater Res 17(01):224–233. doi:10.1557/JMR.2002.0032

Tsui TY, Oliver WC, Pharr GM (1996) Influences of stress on the measurement of mechanical properties using nanoindentation: part I. experimental studies in an aluminum alloy. J Mater Res 11(03):752–759. doi:10.1557/JMR.1996.0091

Uchic MD, Dimiduk DM, Florando JN, Nix WD (2004) Sample dimensions influence strength and crystal plasticity. Science 305(5686):986–989. doi:10.1126/science.1098993

Wang L, Bei H, Gao YF, Lu ZP, Nieh TG (2011) Effect of residual stresses on the hardness of bulk metallic glasses. Acta Mater 59(7):2858–2864. doi:http://dx.doi.org/10.1016/j.actamat.2011.01.025

Windischmann H (1987) An intrinsic stress scaling law for polycrystalline thin films prepared by ion beam sputtering. J Appl Phys 62(5):1800–1807

Withers PJ, Bhadeshia HKDH (2001) Residual stress. Part 1—Measurement techniques. Mater Sci Technol 17(4):355–365

Ye J, Shimizu S, Sato S, Kojima N, Noro J (2006) Bidirectional thermal expansion measurement for evaluating Poisson's ratio of thin films. Appl Phys Lett 89(3):031913